Renewable Energy 209 (2023) 677–688

Contents lists available at ScienceDirect

Renewable Energy

journal homepage: www.elsevier.com/locate/renene

Modeling the acoustic noise from a wave energy converter farm and its impact on marine mammals at the PacWave South site, offshore Newport Oregon

Jennifer L. Harding [a,*], Leiph A. Preston [a], Erick Johnson [b], Jesse D. Roberts [a], Craig A. Jones [c], Kaus Raghukumar [c], Erin Hafla [b]

[a] Sandia National Laboratories, Albuquerque, NM, USA
[b] Montana State University, Bozeman, MT, USA
[c] Integral Consulting, Santa Cruz, CA, USA

ARTICLE INFO

Keywords:
Hydroacoustic modeling
Marine mammal impact
Wave energy converters
Acoustic impact metrics
Effective signal level

ABSTRACT

Marine hydrokinetic devices, such as wave energy converters (WECs), can unlock untapped energy from the ocean's currents and waves. Acoustic impact assessments are required to ensure that the noise these devices generate will not negatively impact marine life, and accurate modeling of noise provides an *a priori* means to viably perform this assessment. We present a case study of the PacWave South site, a WEC testing site off the coast of Newport, Oregon, demonstrating the use of ParAcousti, an open-source hydroacoustic propagator tool, to model noise from an array of 28 WECs in a 3-dimensional (3-D) realistic marine environment. Sound pressure levels are computed from the modeled 3-D grid of pressure over time, which we use to predict marine mammal acoustic impact metrics (AIMs). We combine two AIMs, signal to noise ratio and sensation level, into a new metric, the effective signal level (ESL), which is a function of propagated sound, background noise levels, and hearing thresholds for marine species and is evaluated across 1/3 octave frequency intervals. The ESL model can be used to predict and quantify the potential impact of an anthropogenic signal on the health and behavior of a marine mammal species throughout the 3-D simulation area.

1. Introduction

Marine Hydrokinetic devices (MHKs) are a promising source of renewable energy, converting ocean wave and current kinetics into electricity via wave energy converters (WECs) and current energy converters (CECs), respectively. The estimated marine energy resource in the United States that can be extracted by these technologies is 2300 TWh/yr, which is 57% of the total generated electricity in the United States in 2019 [1]. Much of this untapped resource is from waves, especially on the western United States coast, which account for 1400 TWh/yr alone [1]. Significant permitting hurdles for the installation of MHK devices exist, including the evaluation of the impact these devices have on the surrounding marine life [2,3]. One such impact is the mechanical noise that MHK devices produce, where the frequency content and amplitude of the acoustic noise varies both with the specific type and model of the device [4,5] and with environmental factors like significant wave height [6,7].

Noise levels in the ocean are a growing concern, and anthropogenic noise sources, such as shipping traffic, have been found to negatively impact marine life [8]. Moreover, the ocean acts as a waveguide [9,10] causing sound to travel great distances and expanding the area of impact for anthropogenic sound sources. While the noise produced by MHK devices is less than that of shipping traffic by tens of dB and seismic airguns by ~100 dB (e.g. Ref. [10], for instance, there is a lack of direct observations of MHK noise and MHK array noise. It is therefore imperative to investigate MHK devices as a source of hydroacoustic noise and determine potential resulting impacts on local marine life by considering the devices' unique acoustic signatures, site-specific marine environmental properties such as bathymetry and sound speed (e.g. Ref. [9], and the presence of marine species endemic to an area (e.g., Ref. [11].

To predict how MHK noise propagates in marine environments, short of device installation and observation, we rely on predictions made from hydroacoustic modeling. Modeling the acoustic noise produced by MHK devices allows for the determination of potential marine life impact

* Corresponding author.
E-mail address: jlhardi@sandia.gov (J.L. Harding).

https://doi.org/10.1016/j.renene.2023.04.014
Received 6 December 2022; Received in revised form 10 March 2023; Accepted 4 April 2023
Available online 7 April 2023

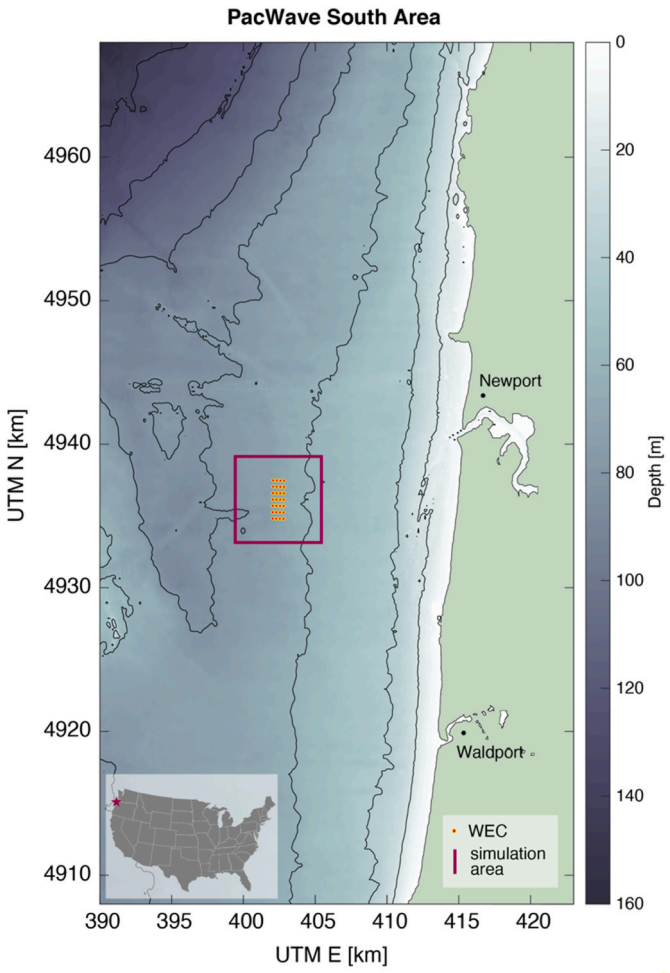

Fig. 1. This map of the PacWave South case study area shows the bathymetry, with contours every 20 m (black lines), the ParAcousti simulation area (maroon box), and the simulated WEC locations (red and yellow heptagrams). Inset shows the location of the PacWave South site offshore Newport, OR (maroon star).

before device installation, thereby reducing the regulatory barriers. Here we simulate and model the acoustic noise in a complex, 3-D marine environment using the open-source software package ParAcousti [12]. ParAcousti is a sophisticated time-domain modeling tool, that uses the linearized velocity-pressure equations to propagate noise sources in a complex, 3-D domain with varying sound speed, density, and seafloor bathymetry.

We simulate the acoustic noise from an array of WEC – modeled after real WEC noise measurements – at the PacWave South site, a future WEC test site off the coast of Newport, Oregon (Fig. 1). Using the PacWave South site as a case study, we demonstrate how ParAcousti can be used to model the 3D sound pressure level (SPL) as well as marine mammal acoustic impact metrics (AIMs). The methodologies here can be applied to other potential MHK installation locations, device technologies, array sizes, and environmental conditions to be incorporated into acoustic impact assessments. While we present our modeling results of the PacWave site, the goal of this case study is largely to demonstrate methodologies and not to make any specific determinations of marine mammal behavioral impacts nor mitigation recommendations.

Sections 1.1, 1.2, and 1.3 provide background of hydroacoustic modeling, the PacWave site, and marine mammal acoustic impact metrics. We detail our methods for hydroacoustic modeling and computation of impact metrics for marine mammals in Section 2. Section 3 presents results from our hydroacoustic modeling of the PacWave site with examples of computation of marine mammal impact metrics. We summarize and make concluding remarks in Section 4.

1.1. Hydroacoustic modeling

There are a variety of methods to model noise propagation that range in complexity and accuracy, from 1-D transmission loss calculations and 2-D parabolic equation approximations to 3-D finite element acoustic modeling software with near-field nonlinear capabilities [13] and references therein). While 1-D methods are simple and quick to execute, they are less accurate because they don't consider factors like bathymetry and ocean properties like sound speed and bottom attenuation, broadband sound, nor noise sources that vary over time and/or space. On the other end of the spectrum, 3-D finite element, nonlinear acoustic propagation software is the most accurate tool available but is computationally intensive and requires time and expertise to perform.

ParAcousti is an open-source software that was specifically developed for MHK acoustic impact assessment applications [12,14] and is more accurate than widely-used 1-D and 2-D methods while less computationally expensive and more user-friendly than its nonlinear finite element counterparts (e.g., COMSOL Multiphysics). ParAcousti can model full waveforms in 3-D and can accurately propagate MHK noise signals in marine environments with complex bathymetry and realistic properties of the seabed, water column, and air-surface interface. This hydroacoustic software suite solves the linearized 3-D velocity-pressure set of coupled first-order partial differential equations in the time domain with fourth-order spatial and second-order temporal accuracy. Any number of sources with broadband frequencies can be modeled within the 3-D simulation domain, and complex sources can be built using combinations of simple physical sources, such as isotropic explosions/implosions or monopole-type forces. Sound pressures, particle velocities, and particle accelerations can be recorded

Table 1
Descriptions of the inputs to and outputs of ParAcousti.

ParAcousti Definitions	Definition Details	This Case Study
3-D gridded simulation domain (netCDF format)	Sound speed model	See Fig. 4a
	Density model	See Fig. 4b
Source parameters	Source type (force, moment)	Force in Z
	Source time function (STF)	See Fig. 3a
	Source location(s)	See Fig. 4c
Algorithm parameters and options	Required: grid size, time step, simulation time, boundary conditions, domain decomposition for parallelization, number of processors	0.7 m grid size, 0.2 ms time step, simulation time of 7 s, absorbing boundary condition, 336 partitions and cores (~10 h wall time and ~147 days of CPU time at 93% efficiency on 2.1 GHz Intel Broadwell E5-2695 v4 processors)
	Optional: attenuation, finite difference operator coefficients	No attenuation, 4th order Taylor series coefficients
Receiver parameters	Receiver type(s) (pressure, particle velocity, particle acceleration)	Pressure
	Receiver location(s)	Grid: 50 × 50 m in North and East and 5 m in depth grid
Output options	Receiver time series, 3-D wavefield, and/or 2-d wavefield time slices	Receiver times series

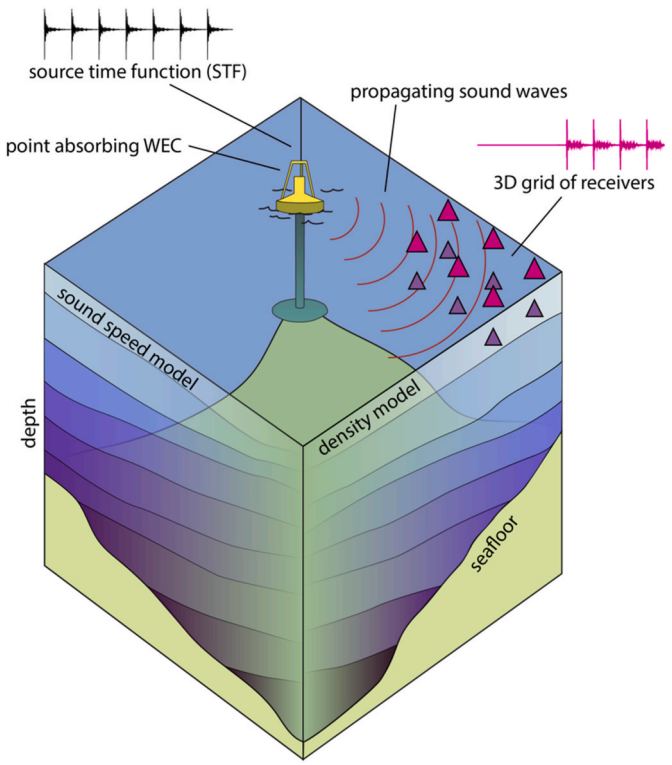

Fig. 2. This diagram represents a cube of ParAcousti simulation domain and shows the inputs required to run the hydroacoustic propagation software. Shown here is a single point absorbing wave energy converter (WEC) producing noise defined by a source time function (STF) and sitting in a marine environment with spatially varying sound speed, density, and bathymetry. A user-defined 3-D grid of receivers (magenta triangles) records the propagating sound waves (red lines) as pressure over the simulation time (magenta time series).

at any set of points within the 3-D domain. See section 2.1 for more details on ParAcousti and its implementation.

Other studies have predicted sound levels due to anthropogenic noise sources in the ocean [14–18], but many don't consider the 3-D complexity of the marine environment, multiple sources (i.e., a WEC array), nor physically model sound as propagating acoustic waves as we show here.

1.2. PACWAVE site

The PacWave test site is a United States Department of Energy-funded, open-ocean wave energy test sites offshore Newport, Oregon run by the University of Oregon (Fig. 1) and is a major facility for wave energy technological research and development. The PacWave South site will be a grid-connected WEC test facility, fully operational in 2023. Because the PacWave South area is well-studied and characterized, it is a good location for a case study demonstrating the application of ParAcousti to a potential WEC installation site. Wave energy resources here have been simulated and hindcasted for 32 years between 1979 and 2010, as per the International Electrotechnical Commission (IEC) requirements [19,20] and the offshore Oregon region has the largest wave heights of the Pacific coast, reaching heights as great as 5 m in the wintertime and 2.3 m in the summertime [20,21]. The PacWave South area also has bathymetric data available [22] (Fig. 1), ocean temperature, salinity, and density predictions from an ocean model, and ambient noise observations [23].

1.3. Marine mammal impact metrics

The greatest perceived risk of WECs to marine life is physical entanglement and collision [24]. Electromagnetic fields generated by WEC devices may also impact marine life (e.g. Refs. [5,25], and references therein). In addition to these risks, there are potential health and behavioral impacts that the hydroacoustic noise produced by WEC devices could have on marine species. [26] concludes that WEC noise is unlikely to affect marine mammals in any capacity, as their WEC noise measurements were only 1–2 dB above the ambient ocean noise. These results, however, are only applicable to the specific location, size and geometry of the WEC devices, and ocean conditions, all of which need to be considered in order to make any conclusions on the potential impact to surrounding marine life for any future WEC installation. Indeed, recent observational studies have concluded that WEC noise could affect marine life behavior [6]. Since presently reported sound levels produced by non-commercial scale WECs (overall maximum of 160 dB re 1 μPa SPL) [6,7,26,27] are well below levels that could harm marine mammal hearing in a temporary or permanent way (overall lowest amongst marine mammal species of 212 dB re 1 μPa peak SPL) [28,29], we focus on the use of marine mammal AIMs for assessing potential behavioral effects. The specific behavioral changes, such as avoidance, for different marine mammal species in relation to different sound levels, however, has not been well quantified [28,30]. With more observational behavioral response studies, sound levels and AIMs can be directly linked to a behavior severity index as is laid out by [11].

Sound is critical to marine life in several ways, including for survival, reproduction, and foraging [31]. The anthropogenic masking of biological and natural sound in the ocean is a growing threat to marine mammals by shrinking communication space, affecting foraging ability, reducing ability to detect predators, and even impairing navigation

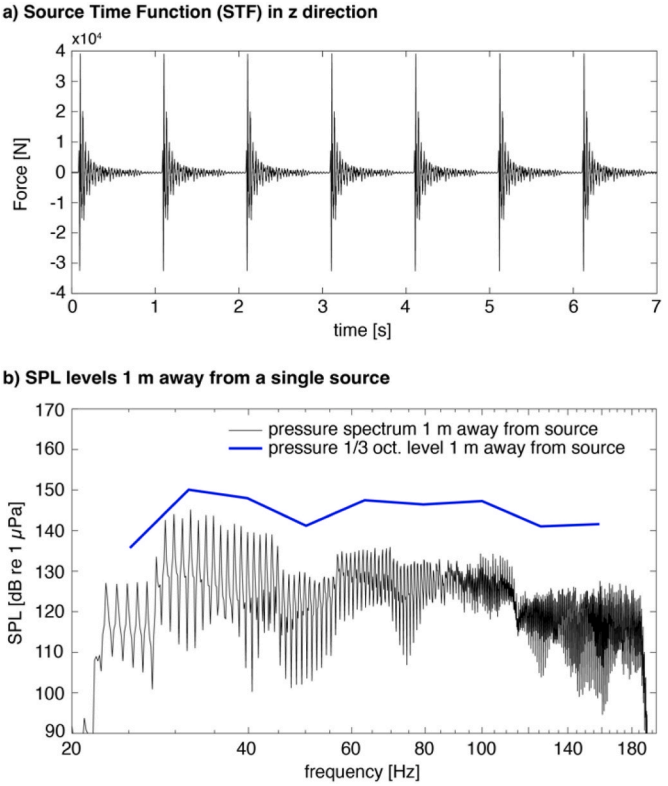

Fig. 3. a) The source time function (STF) emitted by each WEC during the simulation. b) SPL levels from a receiver pressure time series 1 m away from a simulation using a single source, where the black line is the fast Fourier transform of the pressure time series and the blue line is the 1/3 octave SPL level of the pressure time series.

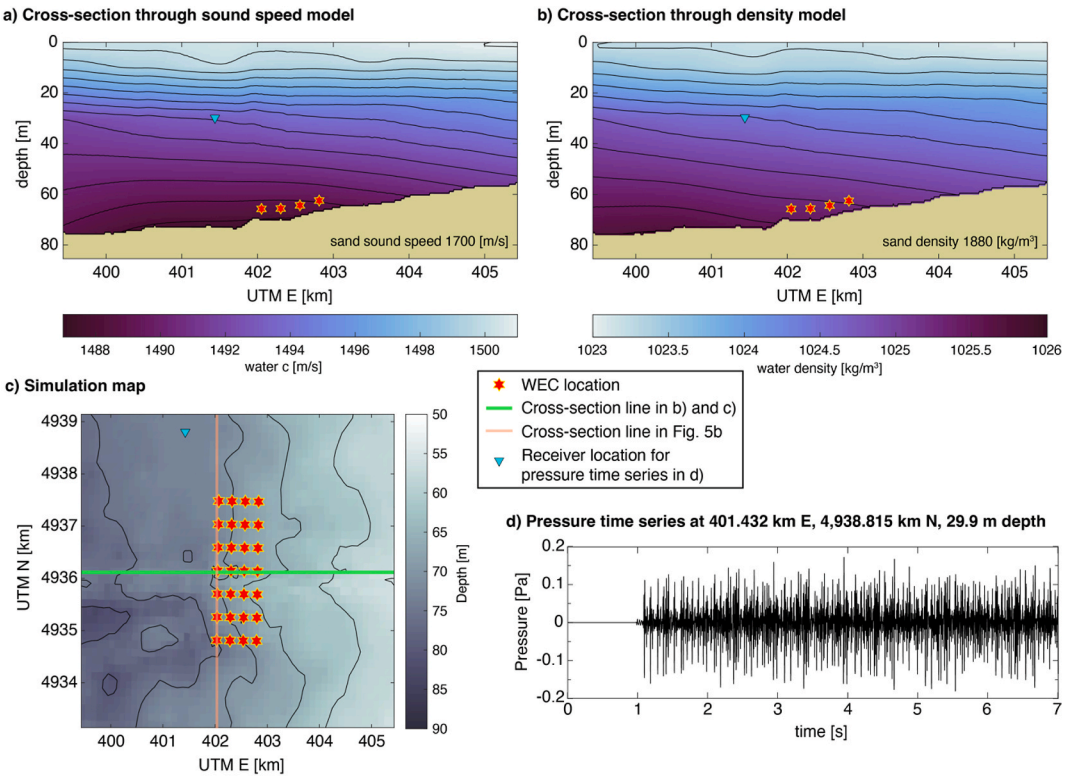

Fig. 4. Cross-sections through the sound speed (a) and density (b) models along the green line in the simulation map in c) show the spatially variable ocean parameters. Sound speed in a) is contoured every 1 m/s, density in b) is contoured every 0.25 kg/m^3, and bathymetry is contoured every 5 m (black lines in (c)), with WEC locations in all panels shown as red and yellow heptagrams. We choose a sandy seafloor with a sound speed of 1700 m/s and density of 1880 kg/m^3, shown as a sand color in a) and b). Cyan triangle shows the projected location in a), b), and c) of the receiver for the pressure time series in d).

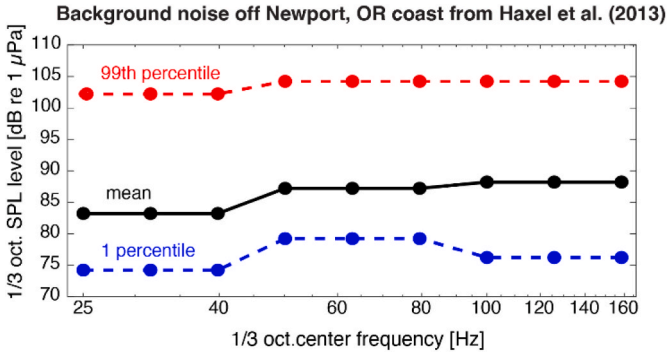

Fig. 5. Background noise observations off the coast of Newport, OR from Ref. [23] that are used in the SNR calculations. Each 1/3 oct. band background noise SPL is plotted as a circle for the mean (black), 1 percentile quietest conditions (blue), and 99th percentile loudest conditions (red).

[32]. Quantifying how an anthropogenic sound source will affect marine life is nontrivial, and requires accurate knowledge of the anthropogenic source, ambient ocean noise, the hearing and perception ability of marine species, and observational data on species' behavioral response to sound stimuli. Because the hearing abilities and behavior responses of marine mammals have been better studied than that of other marine life, like fish, we hereon focus on marine mammal impact [11]. have made significant efforts to establish a framework for assessing marine mammal behavioral response to anthropogenic noise sources, which we follow here. From this framework, will consider two AIMSs: (1) Signal-to-Noise Ratio (SNR), the anthropogenic acoustic signal level relative to the ambient ocean noise levels, and (2) Sensation Level (SnL), the anthropogenic acoustic signal relative to a species' auditory

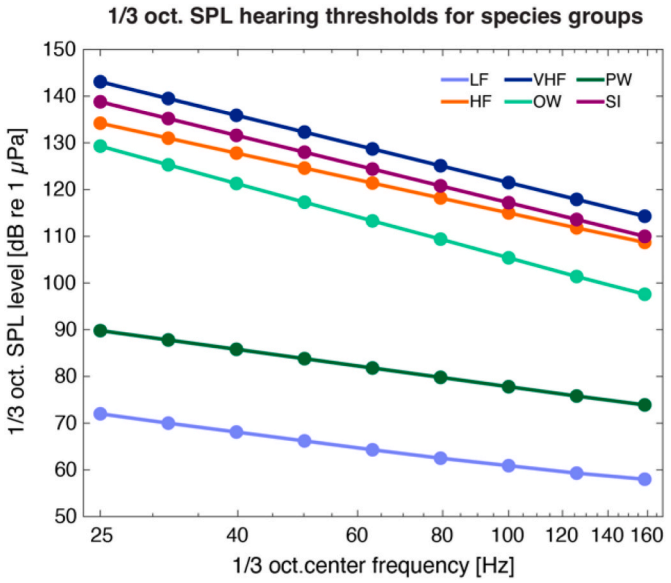

Fig. 6. Hearing thresholds for each marine mammal hearing group [11] at the 1/3 oct. SPL bands considered in this case study (circles).

detection threshold [11,33]. Each of these metrics are considered for each 1/3 octave (oct.) band across the frequency range of the anthropogenic source, reflecting how mammals hear and perceive sound. These two AIMs can then be used to predict how marine mammal behavior might be impacted by an anthropogenic noise source.

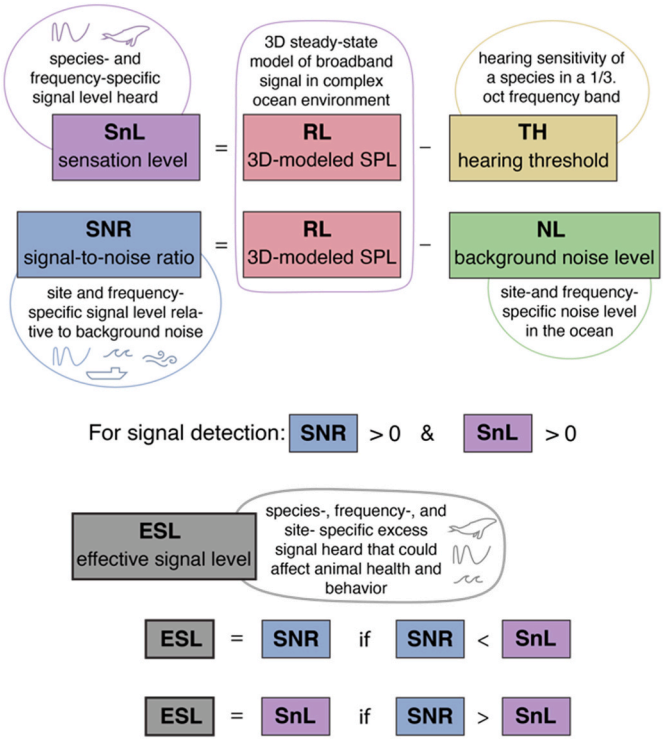

Fig. 7. Diagram describing the marine mammal AIMS SnL, SNR, and ESL and their calculation.

Table 2
Description of the functional hearing species groups; See Ref. [11] for a complete description of genera or species that are included in each hearing group.

Marine Mammal Hearing Group	Description
LF	Low-frequency cetaceans
HF	Mid-frequency cetaceans
VHF	Very high-frequency cetaceans
PW	Phocids in water
OW	Otariids in water
SI	Sirenians

2. Methods

2.1. Modeling sound pressure level with ParAcousti

ParAcousti solves the linear set of velocity-pressure partial differential equations in the time domain using finite difference discretization in a 3-D simulation domain [12,14]. An advantage of time-domain modeling is that any number and/or combination of different noise sources can be modeled simultaneously in a single model run. Inputs to ParAcousti are outlined in Table 1 and Fig. 2 and include values for sound speed and density at every grid node in the simulation domain, a function that defines the acoustic source(s) as a combination of monopole or dipole force(s) and/or moments, the location(s) of noise source (s), and algorithmic parameters such as boundary condition options (i.e. damping sound reflections at domain edges). Output options include pressure, particle velocity, or particle acceleration time series at each user-defined receiver location and instantaneous snapshots of 2-D or 3-D time slices of the wavefield.

We model a 28-WEC array ~11 km off the Oregon coast (Fig. 1) in a 6 × 6 km box in the North and East directions, and 85.4 m in depth, where each WEC independently emits the same broadband signal and is stationary in space. We model our WEC noise source function after measurements made by Ref. [7] of the noise signature from a linear point-source WEC under 1.5 m significant wave height conditions. We choose a source time function (STF) to be a force in the z (vertical) direction with the broadband frequencies reflecting those recorded by Ref. [7] (Fig. 3a). To reduce the computation time, we limit the bandwidth of the WEC noise source signal to 20–198 Hz. Since the modeled WEC source function is generated from the translator moving vertically past the stator, which sits near the seafloor atop a concrete block, we place each WEC source location at 4 m above the seafloor and choose source that has a 1 s periodicity, with the overall 1/3 oct. levels over the entire time series matching the 1/3 oct. SPL levels reported in Ref. [7] (Fig. 3b). The total time length for the STF function should be long enough for the noise to reach the simulation domain edges and reflections to be incorporated, here conservatively chosen to be 7 s so our constant-noise source can reach steady-state everywhere in the simulation domain to later compute SPL.

To define the grid size at which sound speed and density will be defined, we need to consider the highest frequency, f, contained in our STF and the minimum sound speed, c, in our sound speed model. To accurately model the highest frequencies, the grid size, dx, should be defined as $dx = \min(c)/(10 \max(f))$ [12], which in our case is 0.7 m using a minimum sound speed of 1487.5 m/s and maximum frequency of 198 Hz. The time step size, dt, the depends on the grid size and the maximum sound speed in the model, defined by $dt = dx/(2.04 \max(c))$ [12], equal to 0.2 ms for our case study. The STF must be discretized with this time step, and the pressure time series we output will be recorded at integer multiples of this time step (every time step for this work).

We use the predicted density, salinity, and temperature from the Delft3D PacWave ocean model [34], which uses boundary conditions from the Hybrid Coordinate Ocean Model (HYCOM) global operational model [35]. We obtain values for density at every grid node by interpolating the density predictions of the PacWave South area in the water column. We take the temperature and salinity predictions and use the Mackenzie equation to compute the sound speed [36], which we interpolate onto each grid node. Below the seafloor, we chose a density of 1880 kg/m^3 and a sound speed of 1700 m/s to represent sand, which largely covers the seafloor here [37], using bathymetry from a digital elevation model [38]. Ten grid cells around the simulation domain edges are devoted to absorbing boundary conditions. Fig. 4 shows a cross-section through our simulation domain of the density and sound speed models.

We output pressure time series on a grid of 50 × 50 m in the North and East directions and 5 m in depth (see Fig. 4d for a pressure time series example). SPL is then calculated for every receiver location as defined by Equation (1) where P_{RMS} is the root mean square pressure in Pascals (Pa) from the steady state portion of the pressure time series, here from 2 s to 7 s, the end of the time series, and a reference pressure of 1e-6 Pa.

$$SPL = 20\, log\left(\frac{P_{RMS}}{10^{-6}}\right) \quad (1)$$

The broadband SPL of the pressure time series 1 m away from a single WEC in our simulation is 155.61 dB re 1 μPa. Since the signal is periodic, the sound exposure level (SEL) may also be a useful metric, which is defined as the cumulative sum of squared pressures for a 1 s equivalent duration in relation to a reference pressure [11,39]. Since our signal has a 1 s periodicity, the SPL and SEL of our 1 m source level are nearly the same, with a broadband SEL of 155.62 dB re 1 μPa^2-s.

2.2. Computing marine mammal acoustic impact metrics

We compute 3-D models of two marine mammal AIMs, Signal-to-Noise Ratio (SNR) and Sensation Level (SnL) using our 3-D simulation of the acoustic wavefield. SNR describes the signal level (received level) above background levels while SnL describes the signal (received level) relative to a species' hearing threshold, which is akin to a detection

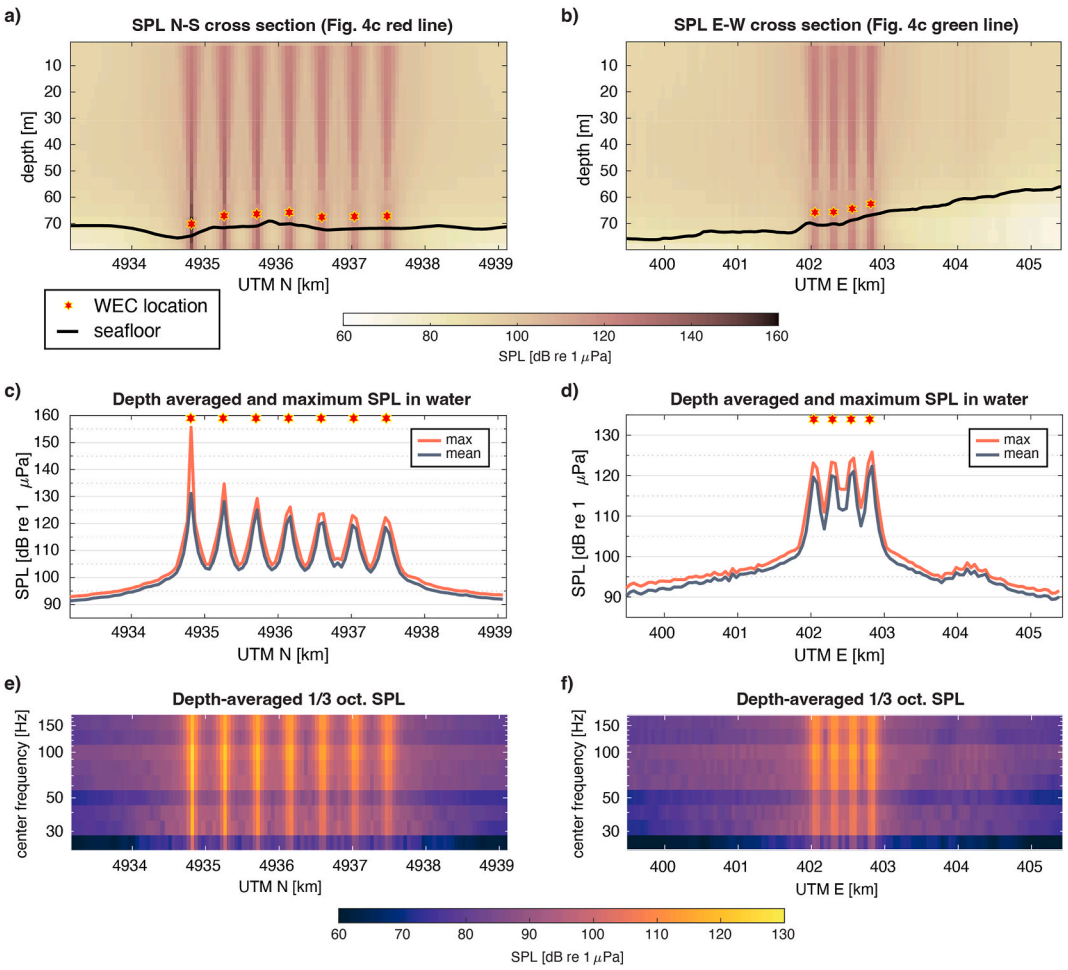

Fig. 8. Top panels a) and b) show 2-D cross-sections through the 3-D SPL model for a N–S line (red line in Fig. 4c) and an E-W line (green line in Fig. 4c). Middle panels show the depth-averaged and maximum SPL in the water column and bottom panels show the 1/3 oct. band depth-averaged SPL for the above SPL cross-sections.

threshold, as described in Fig. 7. Since SNR and SnL are frequency-dependent, we first filter our pressure traces into 1/3 oct. bands, compute 3-D SPL for each 1/3 oct. band, and compute SNR and SnL for each band. To compute SNR, we use the observed background noise measurements from Ref. [23] of the central Oregon coastal area as our noise level (Fig. 5), which we then subtract from our 1/3 oct. SPL models to obtain a mean, 1 percentile (P1), and 99th percentile (P99) 3-D SNR model for each frequency band. To compute SnL, we subtract the hearing thresholds reported in Ref. [11] (Fig. 6) from our 1/3 oct. SPL models to obtain 3-D SnL models for each species group at each frequency band. Table 2 shows the species groups considered here, which have been grouped based on common hearing ability after [11]. While all species groups may not be commonly present at the PacWave site area, we have included them all for demonstrative purposes.

We introduce a new AIM that combines SNR and SnL into an effective signal level (ESL) to determine if a signal has the potential to be detected and is frequency-, location-, and species-dependent. ESL, as outlined in Fig. 7, is set equal to the lesser of the two AIMS SNR and SnL for each 1/3 oct. band. That is, the ESL is equal to SnL if the hearing threshold is higher than the background noise level (i.e. the background noise is not detectable) and equal to the SNR if the background noise level exceeds the hearing threshold (i.e. the background noise level is detectable). If the ESL is greater than zero, then a particular species group at a certain location in a specific 1/3 oct. frequency band can detect the signal. If the ESL is less than zero, then the species group cannot detect the signal at the frequency and location.

3. Results and discussion

3.1. 3D sound pressure level

The predicted 3-D SPL shows the highest SPLs nearest and above each WEC location, reaching 156 dB, and decreasing rapidly in the lateral directions once outside of the array to ~100 dB–200 m away at near-WEC depths and at ~400 m away at shallower ocean depths. At distances greater than ~200 m outside the WEC array, SPLs decay more slowly to, on average, 92 dB–2.3 km away near the edge of the simulation domain. Fig. 8 shows two SPL cross-sections along with the depth-averaged and maximum SPL in the water column and depth-averaged 1/3 oct. SPL for each cross-section. The depth-averaged SPL is defined as the SPL computed using the arithmetic mean of the root-mean-squared pressure (Prms) in the water column, and the maximum SPL is the SPL computed using the maximum Prms in the water column, noting that as the water column increases and decreases in thickness there are more or fewer receivers, respectively.

The SPL results demonstrate how a particular WEC array geometry in a realistic marine environment, where the density and sound speed of the water and the bathymetry spatially vary, produces a unique 3-D acoustic environment. An example of bathymetry causing a local sound heterogeneity can be observed in the SPL model cross-section in Fig. 8b,d where a small canyon likely causes a focusing of sound and a local increase of SPL by several dB ~1 km east of the array towards the shoreline. This SPL model also shows how the WEC noise quickly

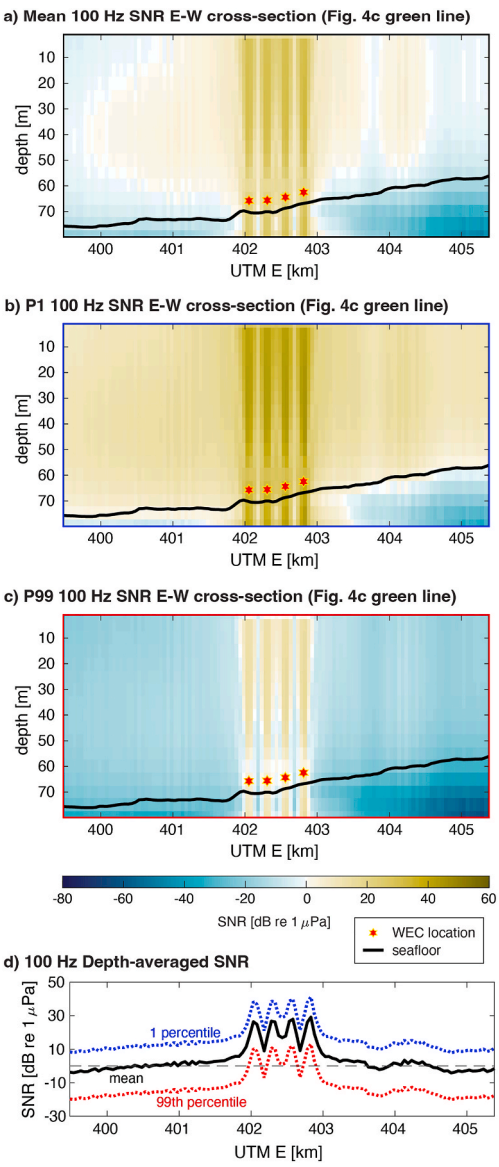

Fig. 9. E-W cross-sections through the 1/3 oct. 100 Hz band 3-D SNR fields using the mean (a), 1 percentile (P1) quietest (b), and 99th percentile (P99) noisiest (c) background noise measurements from Ref. [23]. The depth-averaged SNR for each cross-section in the water column for the above cross-sections are shown in (d).

decreases away from individual WECs, with maximum and mean SPL sharing similar values at the domain extents, ~93 and ~92 dB, respectively.

The variation in the peak SPL nearest each WEC is a result of the receiver grid locations not directly overlapping with the WEC array spacing. In Fig. 8c, the depth-averaged and maximum SPL in the water column near the leftmost (southmost) WEC is much higher than the other WECs because there is a receiver much closer (1 m distance) to this WEC than the others. While every WEC is producing the same 1 m level of sound of 156 dB, the SPL decreases quicky enough from each individual WEC that the 50 m receiver spacing doesn't capture these sharp changes nor the true SPL peaks nearest every WEC. This is a potential pitfall where true peaks could be missed during modeled or real data collection. Potential ways to overcome this pitfall include increasing the receiver grid spacing close to the source(s) or adding additional receivers at 1 m distances from the source(s).

3.2. Marine mammal acoustic impact metrics

From the computed 3-D SPL fields we compute 3-D SNR for each 1/3 oct. frequency band and three background noise percentiles as well as 3-D SnL for each 1/3 oct. frequency band and species group. Fig. 9 shows an E-W cross-section through the 3-D SNR field at the 100 Hz-centered frequency band, which is calculated by subtracting the mean, P99, and P1 background noise level values from the 100 Hz 1/3. oct. SPL. The depth-averaged SNR plot in Fig. 9d shows that the mean SNR falls below zero ~1.5 km from the edge of the WEC area. For the P1 background noise case, representing the quietest conditions, the SNR does not fall below zero anywhere in the simulation domain, whereas the P99 SNR representing the loudest background conditions, falls below zero ~100 m outside the WEC array. Fig. 10 shows the same E-W cross-section through the 3-D SnL field at 100 Hz for each species group, which are calculated by subtracting each species group's hearing threshold at 100 Hz from the 100 Hz 1/3 oct. SPL. The LF and PW groups are sensitive to the 100 Hz signal throughout the cross-section, whereas the HF, VHF, and SI groups have a depth-averaged SnL below zero for the whole cross-section area.

Plan view maps of the depth-averaged SNR and SnL around the WEC array visualize what can be heard by marine species within different 1/3 oct. frequency bands. Fig. 11 shows the depth-averaged SNR in the water column for the entire simulation domain for three background noise states at the 100 Hz 1/3 oct. frequency band. For mean background noise conditions, the 100 Hz depth-averaged SNR drops below zero ~1 km outside of the WEC array. For the P1 quietest background noise conditions, however, our simulation domain is not large enough to capture where the 100 Hz depth-averaged SNR drops below zero and is ~10 dB along the edges of the simulation domain. For the P99 loudest background noise conditions, the 100 Hz depth-averaged SNR is only above zero ~100 m around each individual WEC. Using maximum SPL values in the water column (e.g., red line in Fig. 8c and d) to calculate SNR maps is also possible, which generally increases SNR values by 1–2 dB away from the WEC array, increasing the estimate of maximum distance at which the signal is above background noise by ~500 m for the mean background noise case.

The depth-averaged SnL in the 100 Hz 1/3 oct. frequency band for each species group is shown in Fig. 12. These maps exemplify how the differing hearing thresholds for each species at the same 1/3 oct. hearing band affect the resultant SnL. The LF group, for instance, has a lower hearing threshold and higher 100 Hz depth-averaged SnL values than the SI group, which has a higher hearing threshold and overall lower 100 Hz depth-averaged SnL values. The LF and PW groups are the only two species groups for which the 100 Hz depth-averaged SnL does not fall below zero within the simulation domain. For the rest of the species groups, the 100 Hz depth-averaged SnL falls below zero within ~100 m from each individual WEC. Maps of the depth-average SnL for the LF species group across the nine 1/3 oct. frequency bands modeled are shown in Fig. 13, which demonstrate how the WEC noise source levels and LF hearing thresholds vary across frequency bands and contribute to unique depth-averaged SnL maps.

The ESL is computed by choosing the lesser of the SNR and the SnL AIMs at each 1/3 oct. band for each species group and background noise combination and provides one metric that predicts whether a species can detect the WEC array signal in the 3-D simulation domain. All species groups are found to have a positive ESL and detect the WEC signal within 40 m distance directly above a WEC device. Fig. 14 shows an example calculation of the maximum ESL in the water column for the LF group at the 50 Hz band and P1 quietest background noise conditions. Given that the hearing threshold does not change in space and that we are using the same background noise levels throughout the simulation area, the ESL is always equal to either the SNR or the SnL in the entire domain for this case study. If, however, the background noise levels varied in space, then the ESL would potentially be equal to the SNR in certain parts of the simulation domain and SnL in other parts.

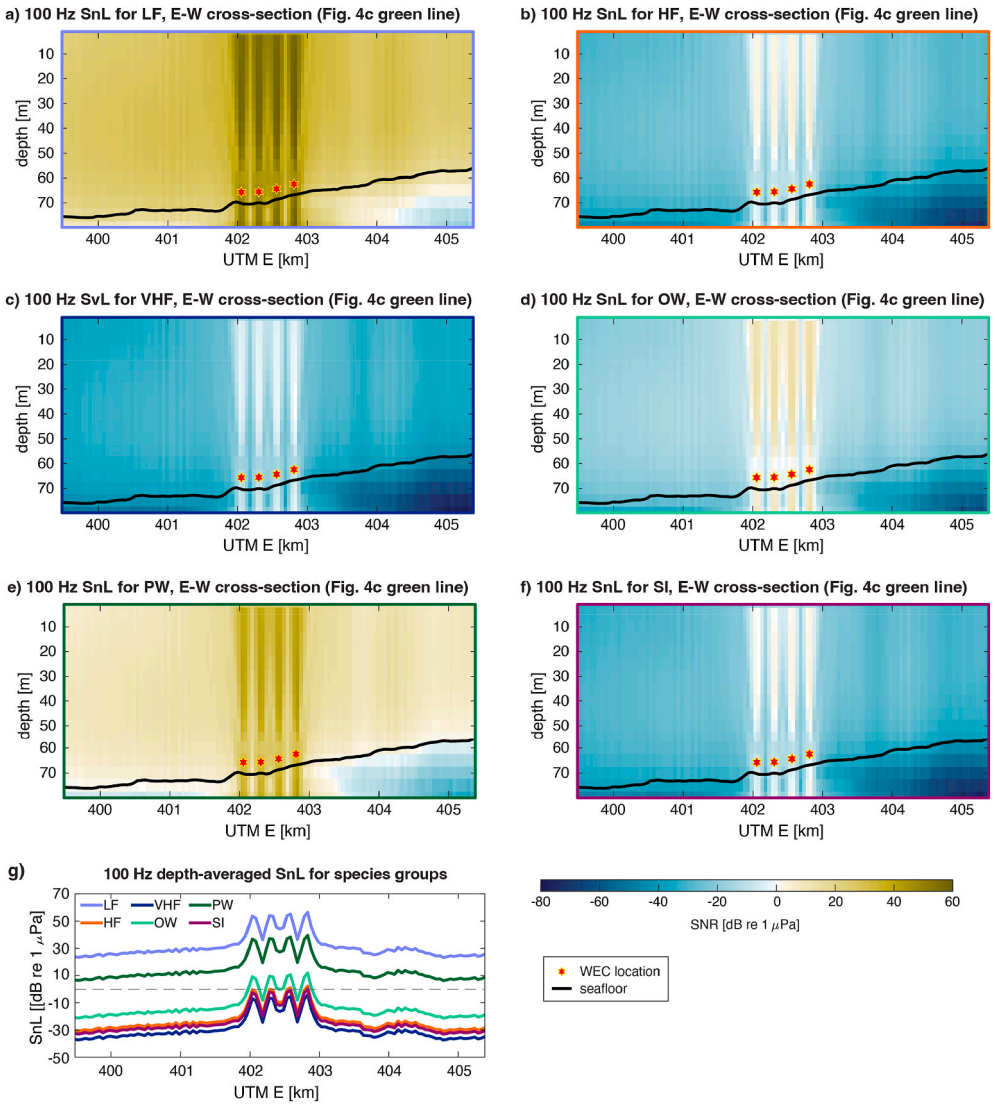

Fig. 10. E-W cross-sections through the 100 Hz 1/3 oct. band SnL fields for each species group (a–g) and the depth-averaged SnL in the water column for those model cross-sections (h).

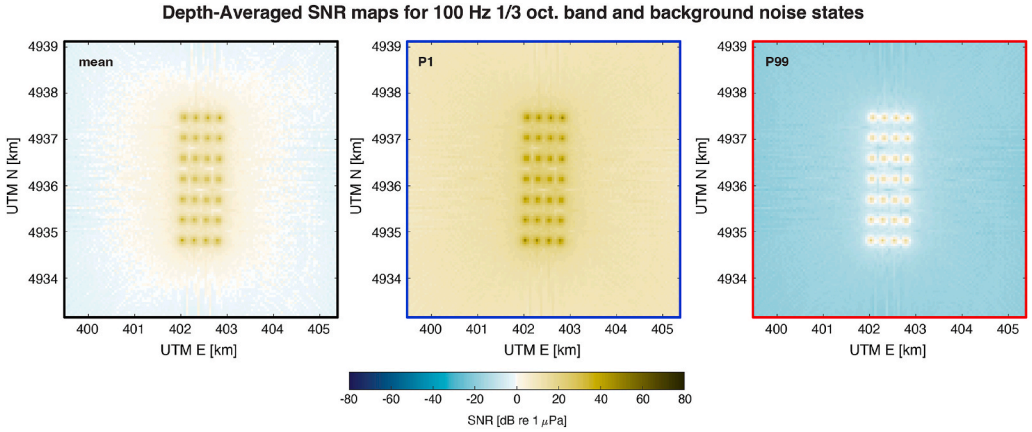

Fig. 11. Maps of depth-averaged SNR in the water column in the 100 Hz 1/3 oct. frequency band for mean background noise conditions (left), 1 percentile (P1) quietest background noise conditions (middle), and 99th percentile (P99) loudest background noise conditions.

The ESL models complement and contextualize the SPL results by showing where in the simulation domain the WEC array signal is detectable to a certain species group in a given frequency band with certain background noise conditions, and therefore where in space a marine mammal has the potential to respond to, or change behavior due to, the WEC array noise. 2-D ESL maps can be produced by using the

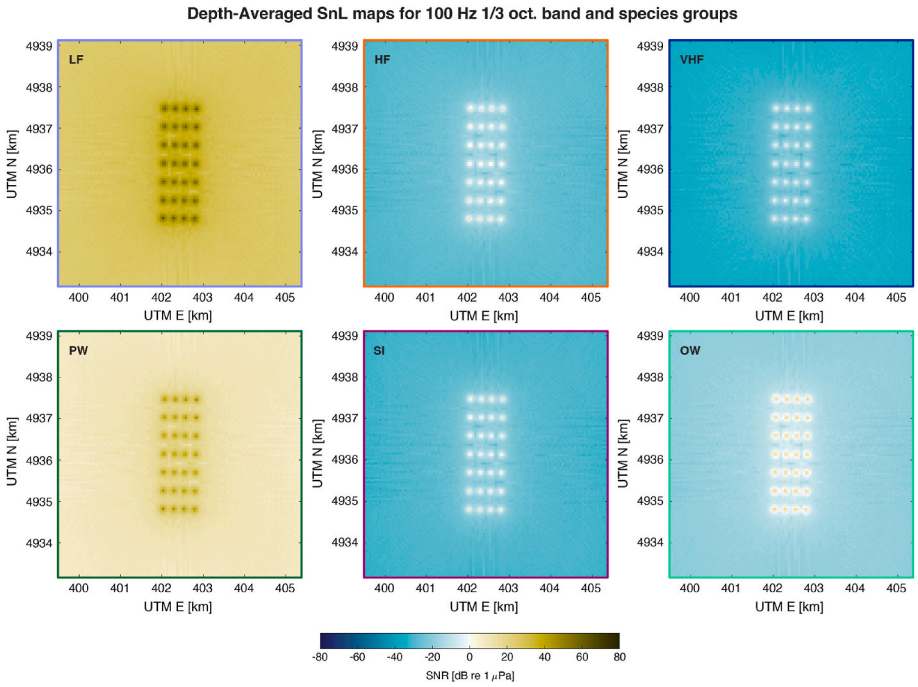

Fig. 12. Maps of depth-averaged SnL in the water column in the 100 Hz 1/3 oct. frequency band for the six marine mammal hearing groups considered in this study (see Table 2). LF-low frequency cetaceans; HF-high-frequency cetaceans; VHF-very high-frequency cetaceans; PW-phocids in water; SI-sirenians; OW-otariids in water. Color bar reflects the overall minimum and maximum depth-averaged SNR and SnL for all results (i.e. combinations of species groups, background noise levels, and frequency bands).

depth-averaged SPL, signifying the noise level a marine mammal might hear, or by using the maximum SPL, which might be useful for assessing the loudest signal a marine mammal could experience and potentially respond to. The ESL can then be further evaluated and compared to observations of marine mammal behavior in different sound conditions to link ESL predictions to behavioral risks, such as is presented in Ref. [11].

For many combinations of species groups, frequency bands, and background noise levels, our simulation domain fully captures the areas where the ESL is greater than zero, and therefore, where the WEC array signal in the water column is detectable and where it is not. Some combinations of species groups, frequency bands, and background noise levels, however, yield ESL models that don't fall below zero within the simulation domain, and thus our present simulation doesn't provide spatial limits on where a species can detect the signal. For example, the low-frequency cetacean (LF) group can hear the WEC array noise on average in the water column, throughout the entire simulation area for 1/3 oct. frequency bands above 25 Hz and in P1 quietest background noise conditions. For mean and loudest background noise conditions at frequency bands above 25 Hz, the ESL is equal to the SNR, which falls below zero within the simulation area. For the quietest background noise conditions, however, both the SNR and SnL fields above 25 Hz, and thus the ESL models, maintain positive values at the edges of the simulation area.

Since the required domain size may not be known *a priori* and larger simulation domains that fully capture the positive ESL area may be computationally infeasible for other studies, there are simple techniques to potentially address these shortcomings. One such technique is to linearly extrapolate the SPL model out to sufficient distances that capture the full positive ESL area, since the SPL has a fairly linear decay away from the WEC array at distances greater than ~500 m (see Fig. 8c and d). Another option is to port the pressure time series or SPL values from the edges of the simulation domain into another modeling tool to simulate pressures or SPLs out to the desired distance from the WEC array.

An important consideration in acoustic impact assessments is the potential physical harm to marine mammals from interaction with a WEC. For this reason, it is important to determine whether the WEC signal can be detected on the whole for each marine mammal in various background noise conditions. Through modeling, such as shown here, the ESL near each WEC can be computed for each 1/3 oct. frequency band, and if just one of the ESL values across the full hearing range of the species is above zero, then the signal is potentially detectable and the devices could be avoided. If every ESL value across the full hearing range for a species is less than zero, then the WEC device sound is undetectable, and with the loss of one sensory input there is a greater potential for physical interaction. Fig. 15 shows an example of the ESL computed from a value of SPL at ~30 m depth above the southmost WEC source in the N–S cross-section shown in Fig. 8a for all frequency bands modeled here and for two species groups at different background noise levels. Despite not including higher frequencies in this study, the WEC noise at this depth can be detected by all species groups considered, even the VHF group with poorer hearing ability at lower frequencies. At shallower depths where the SPL above each WEC source is smaller, however, the ESL for the VHF group is not positive at any of the 1/3 oct. bands modeled in this case study, but would likely be positive if higher frequencies were included in the WEC source.

A limitation of this case study in replicating a realistic scenario stems from the source time function we use, which is associated with a particular significant wave height (1.5 m), does not incorporate variations in operational conditions or signal phase across the WEC array, and is capped at 198 Hz to manage the number of grid cells and reduce the necessary computational resources. The sound that each WEC emits will vary with significant wave height, has higher frequency content upwards of 1 kHz, and realistically, will have variability in phase compared to other WECs. Moreover, changes in weather can affect significant wave height as well as background noise levels, especially at higher frequencies, which has not been considered in this case study. Further modeling needs to be conducted to better quantify these effects on the soundscape. Other limitations include the stationary nature of the WECs in space, and future modeling efforts can incorporate the spatial motion of the acoustic noise source specific to the WECs device type.

4. Conclusions

We presented a case study demonstrating the use of the ParAcousti to model the broadband acoustic noise generated by an array of 28 WECs at the PacWave south site off the coast of Newport, Oregon. Our simulation

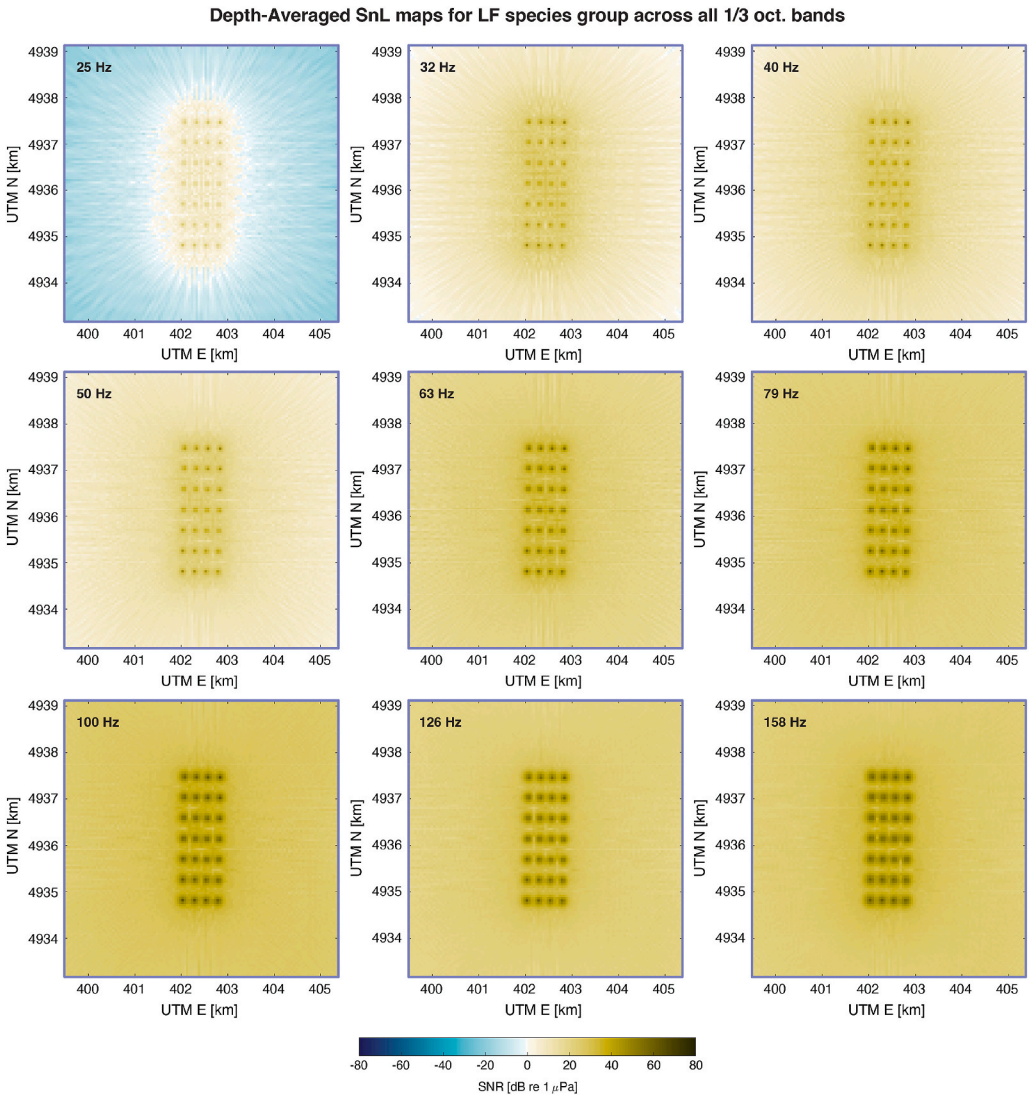

Fig. 13. Maps of depth-averaged SnL in the water column for the LF species group (phocids in water) across the nine 1/3 oct. frequency bands modeled in this study. Color bar reflects the overall minimum and maximum depth-averaged SNR and SnL for all results (i.e. combinations of species groups, background noise levels, and frequency bands).

domain utilized realistic sound speed, density, and bathymetry, all of which affect how sound propagates through a marine environment and impact the modeled acoustic environment. From the grid of simulated pressure over time, we computed 3-D broadband SPL, as well as 1/3 oct. SPL. Using these 1/3 oct. SPL fields, we computed two marine mammal AIMs, SNR and SnL, to quantify how the simulated soundscape could affect different marine species. We also introduced a new AIM called the ESL, which combines the SNR and SnL into one metric of species-specific perception potential that considers the background noise level, frequency band, and a species' hearing ability.

The SPL is highest above each WEC and rapidly decays laterally by 55 dB in ~200 m. At distances greater than 200 m away from the outermost WECs, SPL decays more slowly by 10 dB over ~1.5 km. We found that all species groups can hear the simulated WEC noise within 40 m distance above an individual WEC, where the LF group experiences the loudest signal with an ESL reaching ~80 dB during quietest background noise conditions.

Following the methodology presented here, ParAcousti can be used in acoustic impact assessments to quantify the signal detected by a marine species in a 3-D model space, depth-averaged map, or maximum map. These values can then be referenced to observations of marine mammal behavior in response to an ESL, and can be contextualized within the marine environment's importance to marine mammals (e.g. feeding ground, breeding ground) to assess the signal's risk to a marine mammal species. Moreover, the ESL can be used to determine whether a marine mammal species is able to detect a signal at all, which controls whether an avoidance behavior is possible and the risk due to physical interaction with the device.

Declaration of competing interest

The authors declare that they have no known competing financial interests or personal relationships that could have appeared to influence the work reported in this paper.

Data availability

Data will be made available on request.

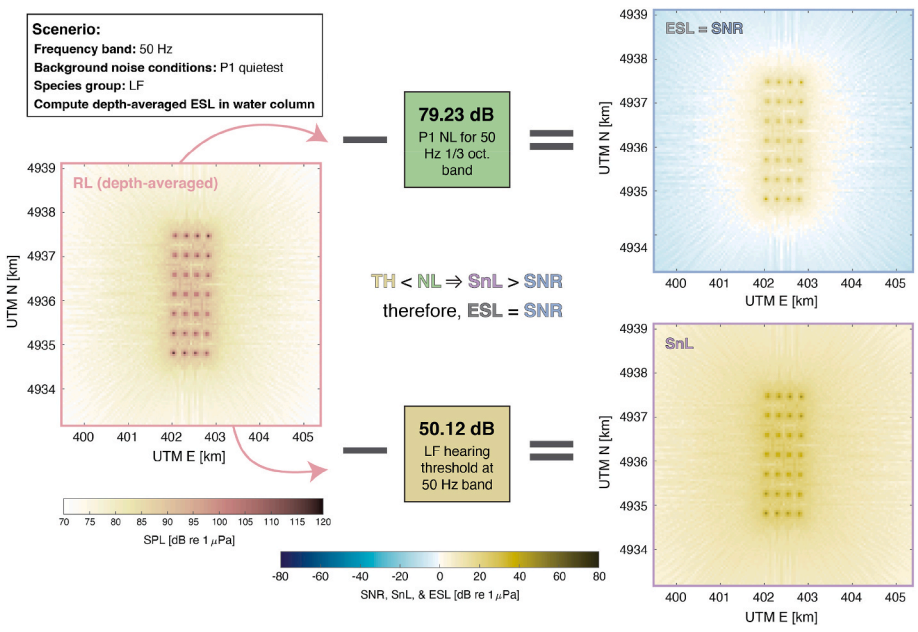

Fig. 14. An example calculation of the depth-averaged ESL in the water column. The scenario considered here is for the 50 Hz 1/3 oct. frequency band, 1 percentile (P1) quietest background noise conditions, and the LF (low-frequency cetaceans) marine mammal hearing group. The received level (RL) is the depth-averaged SPL in the 50 Hz frequency band. The depth-averaged SNR is then RL subtracted by the P1 background noise level (NL) at the 50 Hz frequency band. Depth-averaged SnL is the RL subtracted by the hearing threshold (TH) at the 50 Hz frequency band for the LF group. Since the TH is less than the NL, meaning the LF group can detect the NL, the SnL is then greater than the SNR, and the depth-averaged ESL is therefore equal to the depth-averaged SNR.

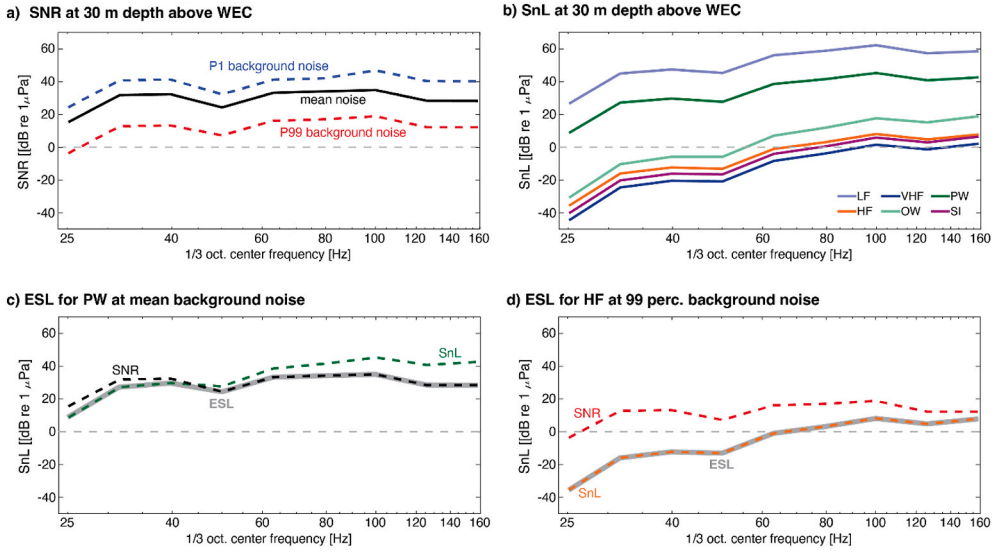

Fig. 15. a) The SNR at 30 m depth above the southwestern most WEC noise source across the nine 1/3 oct. bands for three background noise levels: the mean, the 1 percentile (P1) quietest conditions, and the 99 percentile (P99) loudest conditions. b) the SnL at 30 m depth above the southwestern most WEC noise source across the nine 1/3 oct. bands for the six species hearing groups. c) An example of calculating the ESL (thick gray line) at this point in the simulation area for mean background noise conditions (SNR as black dashed line) and the PW group (SnL as green dashed line). d) An example of calculating the ESL (thick gray line) at this point in the simulation area for P99 background noise levels (SNR as red dashed line) and the HF group (SnL as light green dashed line). For c) and d), the ESL value is equal to the lesser of the two maximum AIMs at each 1/3 oct. band from a) and b). Whether SNR or SnL is smaller can vary across the spectrum depending on the background noise level and the hearing threshold at each 1/3 oct. frequency band, as is shown in c).

Acknowledgements

The authors would like to thank Brandon Southall for his input and guidance. This research was funded by the U.S. Department of Energy's Water Power Technologies Office. This paper describes objective technical results and analysis. Any subjective views or opinions that might be expressed in the paper do not necessarily represent the views of the U.S. Department of Energy or the United States Government. This article has been authored by an employee of National Technology & Engineering Solutions of Sandia, LLC under Contract No. DE-NA0003525 with the U.S. Department of Energy (DOE). The employee owns all right, title and interest in and to the article and is solely responsible for its contents. The United States Government retains and the publisher, by accepting the article for publication, acknowledges that the United States Government retains a non-exclusive, paid-up, irrevocable, world-wide license to publish or reproduce the published form of this article or allow others to do so, for United States Government purposes. The DOE will provide public access to these results of federally sponsored research in accordance with the DOE Public Access Plan https://www.energy.gov/downloads/doe-public-access-plan.

References

[1] L. Kilcher, M. Fogarty, M. Lawson, Marine Energy in the United States: an Overview of Opportunities, National Renewable Energy Laboratory, Golden, CO, 2021. NREL/TP-5700-78773, https://www.nrel.gov/docs/fy21osti/78773.pdf.

[2] R.S. O'Neil, G.J. Staines, M.C. Freeman, Marine Hydrokinetics Regulatory Processes Literature Review, Pacific Northwest National Laboratory, 2019, https://doi.org/10.2172/1591886. PNNL-28608,.

[3] Pacific Energy Ventures, LLC, Handbook of Marine Hydrokinetic Regulatory Processes, United States Department of Energy, Water Power Technologies Office, 2020. DOE-EE-1793.

[4] C. Frid, E. Andonegi, J. Depestele, A. Judd, D. Rihan, S.I. Rogers, E. Kenchington, The environmental interactions of tidal and wave energy generation devices,

Environ. Impact Assess. Rev. 32 (1) (2012) 133–139, https://doi.org/10.1016/j.eiar.2011.06.002.
[5] O. Langhamer, K. Haikonen, J. Sundberg, Wave power—sustainable energy or environmentally costly? A review with special emphasis on linear wave energy converters, Renew. Sustain. Energy Rev. 14 (4) (2010) 1329–1335, https://doi.org/10.1016/j.rser.2009.11.016.
[6] G. Buscaino, G. Mattiazzo, G. Sannino, E. Papale, G. Bracco, R. Grammauta, S. Mazzola, Acoustic impact of a wave energy converter in Mediterranean shallow waters, Sci. Rep. 9 (1) (2019) 9586, https://doi.org/10.1038/s41598-019-45926-1.
[7] K. Haikonen, J. Sundberg, M. Leijon, Hydroacoustic measurements of the noise radiated from wave energy converters in the Lysekil project and Project WESA, in: 1st International Conference and Exhibition on Underwater Acoustics, 2013, pp. 199–209. UA2013 (Corfu, Greece, 23rd-28th June 2013).
[8] C.M. Duarte, L. Chapuis, S.P. Collin, D.P. Costa, R.P. Devassy, V.M. Eguiluz, F. Juanes, The soundscape of the Anthropocene ocean, Science 371 (6529) (2021), https://doi.org/10.1126/science.aba4658.
[9] W. Kuperman, P. Roux, Underwater Acoustics, Springer Handbook of Acoustics, 2007, pp. 149–204.
[10] National Research Council, ocean noise and marine mammals, in: Ocean Noise and Marine Mammals, The National Academy Press, Washington, D.C., 2003.
[11] B.L. Southall, D.P. Nowacek, A.E. Bowles, V. Senigaglia, L. Bejder, P.L. Tyack, Marine mammal noise exposure criteria: assessing the severity of marine mammal behavioral responses to human noise, Aquat. Mamm. 47 (5) (2021) 421–464, https://doi.org/10.1578/AM.47.5.2021.421.
[12] L.A. Preston, Paracousti User Guide. Sandia Report SAND20169291, 2016. Albuquerque, NM, USA.
[13] K.E. Buenau, L. Garavelli, L.G. Hemery, G. García Medina, A review of modeling approaches for understanding and monitoring the environmental effects of marine renewable energy, J. Mar. Sci. Eng. 10 (1) (2022), https://doi.org/10.3390/jmse10010094.
[14] E. Hafla, E. Johnson, C.N. Johnson, L. Preston, D. Aldridge, J.D. Roberts, Modeling underwater noise propagation from marine hydrokinetic power devices through a time-domain, velocity-pressure solution, J. Acoust. Soc. Am. 143 (6) (2018) 3242, https://doi.org/10.1121/1.5039839.
[15] C. Erbe, D.M. Farmer, Zones of impact around icebreakers affecting beluga whales in the Beaufort Sea, J. Acoust. Soc. Am. 108 (3 Pt 1) (2000) 1332–1340, https://doi.org/10.1121/1.1288938.
[16] O.W. Ikpekha, F. Soberon, S. Daniels, Modelling the propagation of underwater acoustic signals of a marine energy device using finite element method, Rev Energy Power Qual J (2014) 97–102, https://doi.org/10.24084/repqj12.246.
[17] K. Rossington, T. Benson, P. Lepper, D. Jones, Eco-hydro-acoustic modeling and its use as an EIA tool, Mar. Pollut. Bull. 75 (1–2) (2013) 235–243, https://doi.org/10.1016/j.marpolbul.2013.07.024.
[18] V.L.G. Todd, L.D. Williamson, J. Jiang, S.E. Cox, I.B. Todd, M. Ruffert, Prediction of marine mammal auditory-impact risk from Acoustic Deterrent Devices used in Scottish aquaculture, Mar. Pollut. Bull. 165 (2021), 112171, https://doi.org/10.1016/j.marpolbul.2021.112171.
[19] International Electrotechnical Commission, Marine Energy - Wave, Tidal and Other Water Current Converters - Part 101: Wave Energy Resource Assessment and Characterization, 2015 (Retrieved from).
[20] W.-C. Wu, T. Wang, Z. Yang, G. García-Medina, Development and validation of a high-resolution regional wave hindcast model for U.S. West Coast wave resource characterization, Renew. Energy 152 (2020) 736–753, https://doi.org/10.1016/j.renene.2020.01.077.
[21] B. Robertson, G. Dunkle, J. Gadasi, G. Garcia-Medina, Z. Yang, Holistic marine energy resource assessments: a wave and offshore wind perspective of metocean conditions, Renew. Energy 170 (2021) 286–301, https://doi.org/10.1016/j.renene.2021.01.136.
[22] NOAA National Centers for Environmental Information, Central Oregon Coastal Digital Elevation Model NAVD 88, 2015. Retrieved from: https://www.ncei.noaa.gov/metadata/geoportal/rest/metadata/item/gov.noaa.ngdc.mgg.dem:11500/html#.
[23] J.H. Haxel, R.P. Dziak, H. Matsumoto, Observations of shallow water marine ambient sound: the low frequency underwater soundscape of the central Oregon coast, J. Acoust. Soc. Am. 133 (5) (2013) 2586–2596, https://doi.org/10.1121/1.4796132.
[24] D.J. Hasselman, D.R. Barclay, R. Cavagnaro, C. Chandler, E. Cotter, D.M. Gillespie, G.J. Staines, Chapter 10: Environmental Monitoring Technologies and Techniques for Detecting Interactions of Marine Animals with Turbines. In *2020 State Of the Science Report*, Pacific Northwest National Lab, 2020.
[25] A.B. Gill, I. Gloyne-Philips, J. Kimber, P. Sigray, Marine renewable energy, electromagnetic (EM) fields and EM-sensitive animals, Mar Renew Energy Technol Environ Interact (2014) 61–79.
[26] J. Tougaard, Underwater noise from a wave energy converter is unlikely to affect marine mammals, PLoS One 10 (7) (2015), e0132391, https://doi.org/10.1371/journal.pone.0132391.
[27] C. Bassett, J. Thomson, B. Polagye, K. Rhinefrank, Underwater noise measurements of a 1/7th scale wave energy converter, in: Paper Presented at the OCEANS'11 MTS/IEEE KONA, 2011 (Waikoloa, HI, USA).
[28] J.J. Finneran, Noise-induced hearing loss in marine mammals: a review of temporary threshold shift studies from 1996 to 2015, J. Acoust. Soc. Am. 138 (3) (2015) 1702–1726, https://doi.org/10.1121/1.4927418.
[29] B.L. Southall, J.J. Finneran, C. Reichmuth, P.E. Nachtigall, D.R. Ketten, A. E. Bowles, P.L. Tyack, Marine mammal noise exposure criteria: updated scientific recommendations for residual hearing effects, Aquat. Mamm. 45 (2) (2019) 125–232, https://doi.org/10.1578/am.45.2.2019.125.
[30] B.L. Southall, Evolutions in marine mammal noise exposure criteria, Acoust. Today 17 (2) (2021), https://doi.org/10.1121/at.2021.17.2.52.
[31] W.W.L. Au, M.C. Hastings, Principles of Marine Bioacoustics, vol. 510, Springer, New York, 2008.
[32] C.W. Clark, W.T. Ellison, B.L. Southall, L. Hatch, S.M. Van Parijs, A. Frankel, D. Ponirakis, Acoustic masking in marine ecosystems: intuitions, analysis, and implication, Mar. Ecol. Prog. Ser. 395 (2009) 201–222, https://doi.org/10.3354/meps08402.
[33] W.T. Ellison, B.L. Southall, C.W. Clark, A.S. Frankel, A new context-based approach to assess marine mammal behavioral responses to anthropogenic sounds, Conserv. Biol. 26 (1) (2012) 21–28, https://doi.org/10.1111/j.1523-1739.2011.01803.x.
[34] K. Raghukumar, S. McWilliams, G. Chang, J. Roberts, C. Jones, Wave energy converter arrays: optimizing power production while minimizing environmental effects, in: Paper Presented at the Offshore Technology Conference, 2019.
[35] E.P. Chassignet, H.E. Hurlburt, O.M. Smedstad, G.R. Halliwell, P.J. Hogan, A. J. Wallcraft, R. Bleck, The HYCOM (HYbrid Coordinate Ocean Model) data assimilative system, J. Mar. Syst. 65 (1–4) (2007) 60–83, https://doi.org/10.1016/j.jmarsys.2005.09.016.
[36] K.V. Mackenzie, Nine-term equation for sound speed in the oceans, J. Acoust. Soc. Am. 70 (1981) 807–812, https://doi.org/10.1121/1.386920.
[37] S.K. Henkel, L.A. Gilbane, Using benthic macrofaunal assemblages to define habitat types on the northeast pacific sedimentary shelf and slope, Estuar. Coast Shelf Sci. 246 (2020), https://doi.org/10.1016/j.ecss.2020.107056.
[38] National Marine Fisheries Service, 2018 Revision to: Technical Guidance for Assessing the Effects of Anthropogenic Sound on Marine Mammal Hearing (*Version 2.0): Underwater thresholds for onset of permanent and temporary threshold shifts*, NOAA Technical Memorandum, 2018. NMFS-OPR-59.
[39] S.B. Martin, C. Morris, K. Broker, C. O'Neill, Sound exposure level as a metric for analyzing and managing underwater soundscapes, J. Acoust. Soc. Am. 146 (1) (2019) 135, https://doi.org/10.1121/1.5113578.